

Kinetic and Mechanistic Investigation of Metallacycle Ring Opening in an Ortho-Metalated Lutetium Aryl Complex

Kevin R. D. Johnson and Paul G. Hayes*

Department of Chemistry and Biochemistry, University of Lethbridge, 4401 University Drive, Lethbridge, Alberta, Canada T1K 3M4

Received August 19, 2010

Reactivity involving metallacycle ring opening of ortho-metalated bis(phosphinimine)carbazolide complexes ($L^{Ph-k^3N, \kappa^2C^{P-Ph}}Lu(THF)$ (**1a**) and ($L^{Pipp-k^3N, \kappa^2C^{P-Ph}}Lu(THF)$ (**1b**); $L = [1,8-(Ph_2P=NAr)_2dmc]$; Ar = Ph (L^{Ph}), *p*-isopropylphenyl (L^{Pipp}); dmc = 3,6-dimethylcarbazolide) is described. Reaction of **1a,b** with bulky anilines (2,4,6-trimethylaniline, MesNH₂; 2,4,6-triisopropylaniline, TripNH₂) promoted metallacycle ring opening of two ortho-metalated *P*-phenyl groups to liberate the bis(anilide) products ($L^{Ph-k^3N}Lu(NHMe)_2$ (**2**) and ($L^{Pipp-k^3N}Lu(NHTrip)_2$ (**3**)). Regardless of the quantity of TripNH₂ or MesNH₂ utilized, double ring opening always prevailed to afford the bis(anilide) product, rather than the mono(anilide). In contrast, reaction of complex **1b** with the bulkier reagent 2,4,6-tri-*tert*-butylaniline (Mes**NH*₂) only caused metallacycle ring opening of one ortho-metalated *P*-phenyl group, affording the mono(anilide) complex ($L^{Pipp-k^3N, \kappa^2C^{P-Ph}}Lu(NHMe^*)$ (**4**)) exclusively. Complex **4** rapidly undergoes an intramolecular rearrangement whereby metalation of an *N*-aryl group promotes metallacycle ring opening of the ligated *P*-phenyl moiety to give ($L^{Pipp-k^3N, \kappa^2C^{N-Pipp}}Lu(NHMe^*)$ (**5**)) as the structural isomer. Through deuterium labeling and kinetic studies it was established that the thermal rearrangement of **4** does not proceed through an imido intermediate. Compounds **2**, **3**, and **5** were characterized by single-crystal X-ray diffraction studies.

Introduction

A decomposition route often encountered in organo-lanthanide complexes is ligand cyclometalation via intramolecular C–H bond activation. Such pathways have been well-documented in highly reactive alkyl and hydrido rare-earth complexes supported by Cp* and Cp' (Cp' = substituted cyclopentadienyl),¹ β-diketiminato,² amido-pyridinato,³ and

anilido-phosphinimine ligands,⁴ in addition to many other scaffolds.

From a synthetic perspective, a ligand metalation process can have diverse consequences. For example, in the context of an olefin polymerization catalyst, the cyclometalative C–H bond activation often results in catalyst deactivation and deprivation of any living polymerization processes.⁵ Furthermore, ligand metalation may occur through numerous competing intramolecular C–H bond activation pathways. If multiple products are generated, it often proves difficult to separate or characterize the mixture.

While frequently unfavorable, ligand metalation processes can sometimes be exploited to achieve a desired form of reactivity.⁶ A recent example reported by Waterman et al. involves a cyclometalated zirconium triamidoamine species that exhibits catalytic reactivity for the selective dehydrocoupling of phosphines and arsines (Scheme 1),⁷ in addition to catalytic hydrophosphination of terminal alkynes.⁸

*To whom correspondence should be addressed. E-mail: p.hayes@uleth.ca.

(1) (a) Evans, W. J.; Ulibarri, T. A.; Ziller, J. W. *Organometallics* 1991, 10, 134–142. (b) Evans, W. J.; Perotti, J. M.; Ziller, J. W. *Inorg. Chem.* 2005, 44, 5820–5825. (c) Evans, W. J.; Champagne, T. M.; Ziller, J. W. *J. Am. Chem. Soc.* 2006, 128, 14270–14271. (d) den Haan, K. H.; Teuben, J. H. *J. Chem. Soc., Chem. Commun.* 1986, 682–683. (e) Booiij, M.; Meetsma, A.; Teuben, J. H. *Organometallics* 1991, 10, 3246–3252. (f) Booiij, M.; Deelman, B.-J.; Duchateau, R.; Postma, D. S.; Meetsma, A.; Teuben, J. H. *Organometallics* 1993, 12, 3531–3540. (g) Thompson, M. E.; Bercaw, J. E. *Pure Appl. Chem.* 1984, 56, 1–11. (h) Takenaka, Y.; Hou, Z. *Organometallics* 2009, 28, 5196–5203.

(2) (a) Conroy, K. D.; Hayes, P. G.; Piers, W. E.; Parvez, M. *Organometallics* 2007, 26, 4464–4470. (b) Hayes, P. G.; Piers, W. E.; Lee, L. W. M.; Knight, L. K.; Parvez, M.; Elsegood, M. R. J.; Clegg, W. *Organometallics* 2001, 20, 2533–2544. (c) Hayes, P. G.; Piers, W. E.; Parvez, M. *Organometallics* 2005, 24, 1173–1183. (d) Knight, L. K.; Piers, W. E.; Fleurat-Lessard, P.; Parvez, M.; McDonald, R. *Organometallics* 2004, 23, 2087–2094. (e) Knight, L. K.; Piers, W. E.; McDonald, R. *Organometallics* 2006, 25, 3289–3292. (f) Kenward, A. L.; Piers, W. E.; Parvez, M. *Organometallics* 2009, 28, 3012–3020.

(3) (a) Luconi, L.; Lyubov, D. M.; Bianchini, C.; Rossin, A.; Faggi, C.; Fukin, G. K.; Cherkasov, A. V.; Shavyrin, A. S.; Trifonov, A. A.; Giambastiani, G. *Eur. J. Inorg. Chem.* 2010, 608–620. (b) Qayyum, S.; Skvortsov, G. G.; Fukin, G. K.; Trifonov, A. A.; Kretschmer, W. P.; Döring, C.; Kempe, R. *Eur. J. Inorg. Chem.* 2010, 248–257. (c) Skvortsov, G.; Fukin, G.; Trifonov, A.; Noor, A.; Döring, C.; Kempe, R. *Organometallics* 2007, 26, 5770–5773. (d) Zimmermann, M.; Estler, F.; Herdtweck, E.; Törnroos, K. W.; Anwander, R. *Organometallics* 2007, 26, 6029–6041.

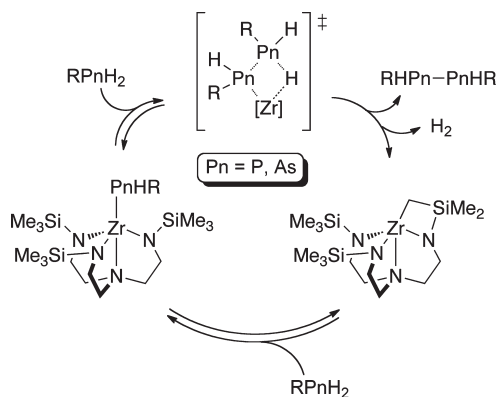
(4) (a) Conroy, K.; Piers, W.; Parvez, M. *J. Organomet. Chem.* 2008, 693, 834–846. (b) Liu, B.; Cui, D.; Ma, J.; Chen, X.; Jing, X. *Chem. Eur. J.* 2007, 13, 834–845. (c) Liu, B.; Liu, X.; Cui, D.; Liu, L. *Organometallics* 2009, 28, 1453–1460.

(5) (a) Schrock, R. R.; Bonitatebus, P. J., Jr.; Schrodi, Y. *Organometallics* 2001, 20, 1056–1058. (b) Schrodi, Y.; Schrock, R. R.; Bonitatebus, P. J., Jr. *Organometallics* 2001, 20, 3560–3573.

(6) (a) Mork, B. V.; Tilley, T. D. *J. Am. Chem. Soc.* 2001, 123, 9702–9703. (b) Mork, B. V.; Tilley, T. D. *J. Am. Chem. Soc.* 2004, 126, 4375–4385.

(7) (a) Roering, A. J.; Davidson, J. J.; MacMillan, S. N.; Tanski, J. M.; Waterman, R. *Dalton Trans.* 2008, 4488–4498. (b) Waterman, R. *Organometallics* 2007, 26, 2492–2494.

(8) Roering, A. J.; Leshinski, S. E.; Chan, S. M.; Shalumova, T.; Macmillan, S. N.; Tanski, J. M.; Waterman, R. *Organometallics* 2010, 29, 2557–2565.

Scheme 1. Mechanism of Pnictogen Dehydrocoupling⁷

Recently, we described the synthesis of a bis(phosphinimine)-carbazolidine pincer ligand, **L** (**L** = [1,8-(Ph₂P=NAr)₂dmc]; Ar = Ph (**L^{Ph}**), *p*-isopropylphenyl (**L^{Pipp}**); dmc = 3,6-dimethylcarbazolidine), and its use in the preparation of well-defined organolutetium complexes.⁹ It was found that dialkyl lutetium complexes of **L** were thermally unstable and rapidly underwent two sequential intramolecular metalative alkane elimination processes. The final product of this transformation contained the ligand bound in a κ^3 manner through the three nitrogen atoms of the ligand framework and two ortho-metalated P-phenyl rings (**L^{Ar}- κ^3 N, κ^2 C^{P-Ph}**)Lu(THF) (Ar = Ph (**1a**), *p*-isopropylphenyl (**1b**)). Herein, we report an investigation into the reactivity patterns of these ortho-metalated organolutetium complexes through the process of metallacycle ring opening. In particular, we prepared bis(anilide) lutetium complexes supported by **L** as well as a mixed aryl/anilide lutetium complex. The latter was assessed for its potential to liberate a lutetium imido complex (LLu=NR) by thermolysis. As a result of this study, novel reactivity patterns were uncovered in conjunction with the clean formation of complexes that exhibit unique bonding modes and structures.

Results and Discussion

Metallacycle Ring-Opening Reactivity. The ortho-metalated lutetium aryl complex **1** can be reacted with various anilines in toluene solution at ambient temperature to give the metallacycle ring-opened product. For example, treatment of **1a** with 2 equiv of 2,4,6-trimethylaniline (MesNH₂) resulted in an immediate reaction whereby ring opening of the metalated P-phenyl rings liberated the bis(anilide) complex **2**, (**L^{Ph}- κ^3 N**)Lu(NHMe)₂ (Scheme 2). Similar reactivity has been previously documented in rare-earth complexes supported by an anilido-phosphinimine ligand.^{4b,c}

The bis(anilide) lutetium complex **2** is C_{2v} symmetric in solution, as depicted by a sharp singlet (δ 30.55) in its ³¹P{¹H} NMR spectrum (benzene-*d*₆). The ¹H NMR spectrum for complex **2** exhibited the expected signals for the ancillary ligand, in addition to a set of resonances corresponding to two mesityl anilide ligands. In particular, the NH anilide protons of complex **2** gave rise to a singlet at δ 3.97 with an integration of 2H (benzene-*d*₆).

Single crystals of complex **2** suitable for an X-ray diffraction study were readily obtained from a benzene solution layered with pentane at ambient temperature. The molecular structure

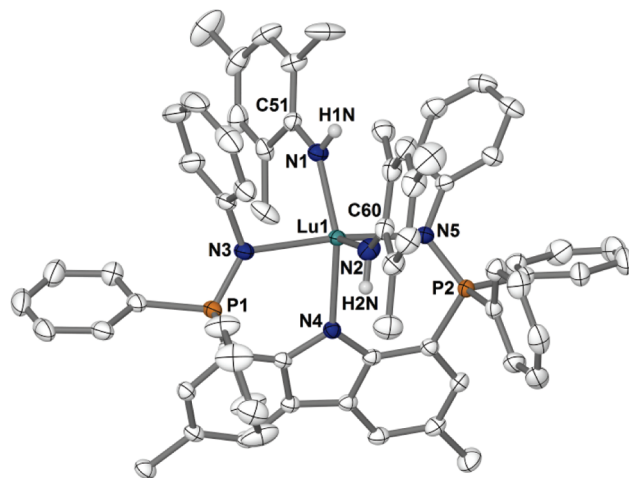
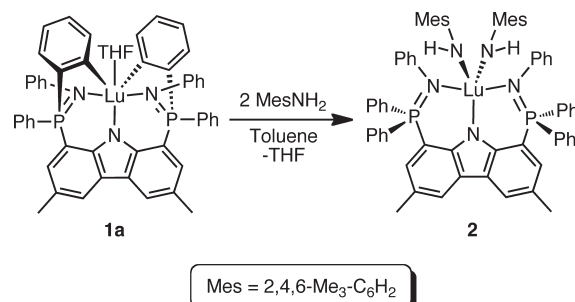


Figure 1. Thermal ellipsoid plot (50% probability) of **2** with hydrogen atoms (except H1N and H2N) and solvent molecules of crystallization omitted for clarity.

Scheme 2. Metallacycle Ring-Opening Reaction of Complex **1a** with MesNH₂

of **2** is illustrated in Figure 1 as a thermal ellipsoid plot. In the solid state, complex **2** is defined by coordination of two 2,4,6-trimethylanilide ligands and the ancillary pincer ligand bound in a κ^3 fashion through its three nitrogen atoms. The five-coordinate lutetium center exhibits a distorted-trigonal-bipyramidal geometry with the anilide ligands (N1 and N2) and N4 of the ancillary in the equatorial positions. The phosphinimine nitrogen donors of the pincer ligand (N3 and N5) occupy the apical sites. The metal center sits above the plane of the dimethylcarbazole backbone by 0.770 Å. The lutetium–anilide bond lengths fall within the normal range at 2.1777(18) Å (Lu1–N1) and 2.1749(19) Å (Lu1–N2) (Table 1). Similarly, the ancillary ligand, **L^{Ph}**, coordinates to lutetium with bond lengths of 2.3586(17) Å (Lu1–N3), 2.3595(16) Å (Lu1–N4), and 2.3586(17) Å (Lu1–N5), which correspond well with previously reported values.⁹

Of particular interest to us was the installation of only one anilide group on lutetium so as to afford a mixed aryl/anilide species. The impetus behind this goal stemmed from the idea that thermolysis of a mixed aryl/anilide complex may promote intramolecular metallacycle ring opening to yield a terminal lutetium imido complex.¹⁰ To this end, we explored the reaction of complex **1a** with only 1 equiv of MesNH₂ in the prospect of generating the mono(anilide) congener of **2**. Unfortunately, repeated attempts of this reaction were

(9) Johnson, K. R. D.; Hayes, P. G. *Organometallics* **2009**, *28*, 6352–6361.

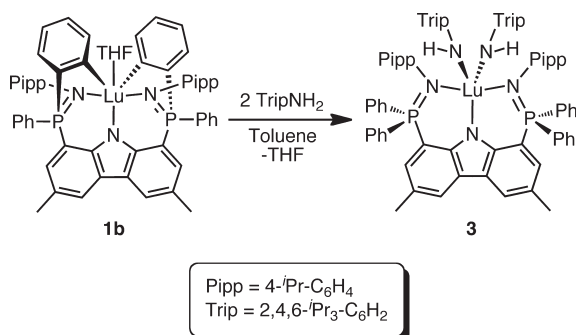
(10) (a) Scott, J.; Basuli, F.; Fout, A. R.; Huffman, J. C.; Mindaola, D. J. *Angew. Chem., Int. Ed.* **2008**, *47*, 8502–8505. (b) Basuli, F.; Tomaszewski, J.; Huffman, J. C.; Mindaola, D. J. *Organometallics* **2003**, *22*, 4705–4714.

Table 1. Selected Bond Distances (Å) and Angles (deg) for Compounds **2** and **3**

	2	3
Lu1–N1	2.1777(18)	2.2030(72)
Lu1–N2	2.1749(19)	2.1698(81)
Lu1–N3	2.3586(17)	2.3309(76)
Lu1–N4	2.3595(16)	2.3225(71)
Lu1–N5	2.3586(17)	2.3394(69)
P1–N3	1.5943(18)	1.5764(83)
P2–N5	1.6097(17)	1.6000(72)
N3–Lu1–N5	168.76(6)	170.75(27)
N3–Lu1–N4	86.38(6)	84.91(26)
N4–Lu1–N5	84.44(6)	86.35(26)
N1–Lu1–N2	118.11(7)	110.07(28)
Lu1–N1–C51 ^a	144.02(15)	
Lu1–N2–C60 ^a	151.34(17)	
Lu1–N1–C57 ^b		146.53(66)
Lu1–N2–C72 ^b		143.77(65)

^aThe listed angle pertains only to complex **2**. ^bThe listed angle pertains only to complex **3**.

Scheme 3. Metallacycle Ring-Opening Reaction of Complex **1b** with TripNH₂



hampered by Schlenk-type ligand redistribution processes whereby only the bis(anilide) complex **2** could be isolated. Similar reactivity has previously been documented in the preparation of other mono(anilide) rare-earth complexes.^{2d}

In a further effort to prepare a mono(anilide) lutetium complex, we pursued the possibility of reacting **1** with anilines of steric bulk even greater than that of MesNH₂. The premise behind this approach was to install a sufficiently bulky anilide ligand to inhibit further intermolecular metallacycle ring opening. Thus, we performed reactions of complex **1** with various anilines of gradually increasing steric bulk; specifically, the reagents 2,4,6-triisopropylaniline (TripNH₂) and 2,4,6-tri-*tert*-butylaniline (Mes**NH*₂) were utilized.

Reaction of complex **1b** with TripNH₂ afforded the double metallacycle ring-opening product ($\text{L}^{\text{Pipp-}\kappa^3\text{N}}\text{Lu}(\text{NHTrip})_2$) (**3**), analogous to the bis(anilide) **2** (Scheme 3). Similar to the case for **2**, complex **3** exhibited C_{2v} symmetry in solution on the NMR time scale. In the ³¹P{¹H} NMR spectrum of **3**, a sharp singlet resonating at δ 30.57 (benzene-*d*₆) was observed. This shift was highly comparable to the ³¹P{¹H} NMR signal for complex **2** (δ 30.55). The ¹H NMR spectrum consisted of the expected resonances for the ancillary ligand as well as signals corresponding to two Trip anilide ligands. Remarkably, the two NH protons for complex **3** were found to resonate with the same chemical shift as complex **2** at δ 3.97 (benzene-*d*₆).

Single crystals of complex **3** were obtained by recrystallization from a concentrated pentane solution at ambient temperature. The solid-state structure of **3**, as determined from an X-ray diffraction experiment, is depicted in Figure 2.

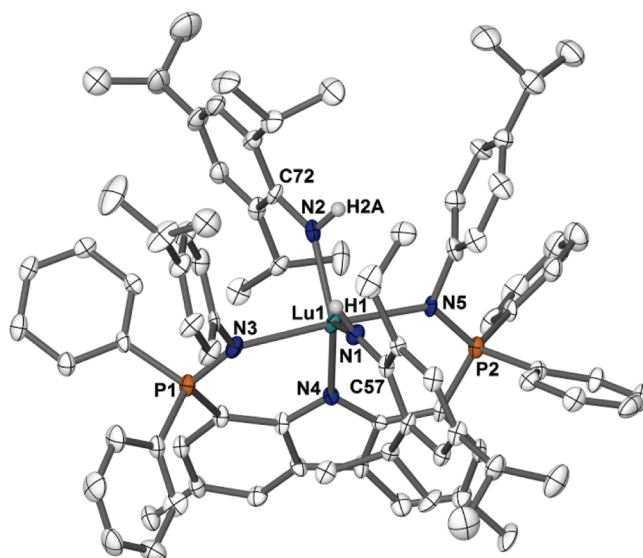


Figure 2. Thermal ellipsoid plot (30% probability) of **3** with hydrogen atoms (except H1N and H2N) and solvent molecules of crystallization omitted for clarity.

Similar to that observed in **2**, the lutetium center in complex **3** adopts a trigonal-bipyramidal geometry with two Trip anilide ligands and the ancillary pincer bound in a κ^3 fashion through its three nitrogen atoms. Likewise, the anilide ligands (N1 and N2) and N4 of the ancillary ligand occupy the equatorial positions, while N3 and N5 define the apical sites. The lutetium–anilide bond lengths in complex **3** are comparable to that of **2** with distances of 2.2030(72) and 2.1689(81) Å for Lu1–N1 and Lu1–N2, respectively (Table 1). In addition, the Lu–N–C anilide bond angles in both complexes **2** and **3** are similar with values ranging from 143.77(65) to 151.34(17)°.

In contrast to the reactivity observed upon reaction of **1** with MesNH₂ and TripNH₂, addition of 1 equiv of 2,4,6-tri-*tert*-butylaniline (Mes**NH*₂) to **1b** only promoted metallacycle ring opening of a single ortho-metallated P-phenyl group, generating the desired mono(anilide) complex ($\text{L}^{\text{Pipp-}\kappa^3\text{N,}\kappa\text{C}^{\text{P-Ph}}}\text{Lu}(\text{NHMe}^*)$) (**4**) (Scheme 4). Even under forcing conditions (100 °C for 24 h) with multiple equivalents of Mes**NH*₂, it was found that double substitution of **1b** (to make ($\text{L}^{\text{Pipp-}\kappa^3\text{N}}\text{Lu}(\text{NHMe}^*)_2$) was not possible.

Interestingly, complex **4** was highly unstable toward a thermally induced intramolecular rearrangement to the structural isomer ($\text{L}^{\text{Pipp-}\kappa^3\text{N,}\kappa\text{C}^{\text{N-Pipp}}}\text{Lu}(\text{NHMe}^*)$) (**5**) (Scheme 4). Unfortunately, the high thermal instability of **4** precluded its isolation as a solid. Complex **4** could, however, be readily observed in situ by ³¹P{¹H} NMR spectroscopy throughout the transformation from **1b** to **5**. The ³¹P{¹H} NMR spectrum of **4** revealed a marked difference from that observed for **2** and **3**. In the solution state, complex **4** exhibited low symmetry (C₁), as demonstrated by two singlets of equal intensity in the ³¹P{¹H} NMR spectrum at δ 31.77 and 22.64 (benzene-*d*₆), corresponding to the chemically inequivalent phosphinimine groups. Attempts to fully characterize **4** in situ by other NMR nuclei (¹H or ¹³C{¹H}) were unsuccessful due to the severity of overlapping signals in the ¹H or ¹³C{¹H} NMR spectra corresponding to complexes **1b**, **4**, and **5**.

The thermal transformation of **4** to **5** liberated a structural isomer whereby the ancillary ligand is ortho-metallated via an N-aryl ring in **5**, as compared to a P-phenyl ring in **4**. The ³¹P{¹H} NMR spectrum of complex **5** contains two resonances

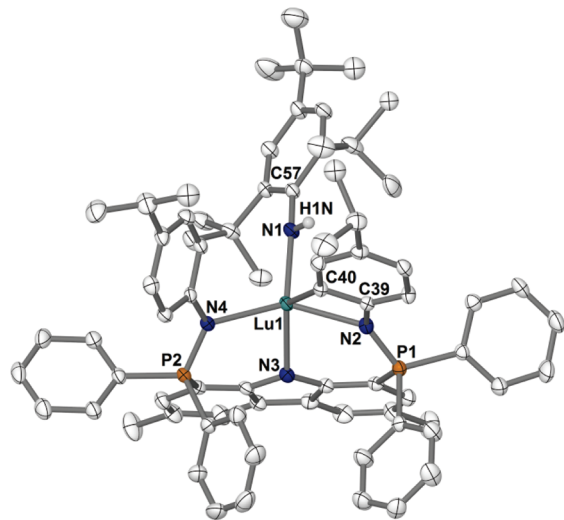
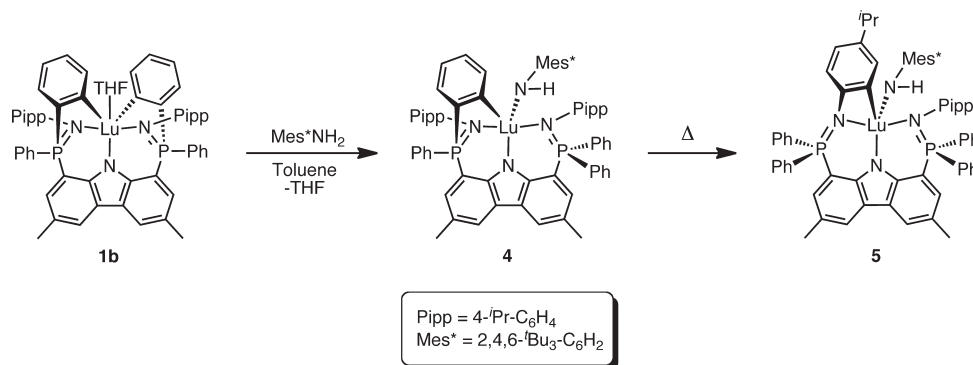
Scheme 4. Metallacycle Ring-Opening Reaction of **1** with 1 Equiv of Mes*NH₂

Figure 3. Thermal ellipsoid plot (50% probability) of **5** with hydrogen atoms (except H1N) and solvent molecules of crystallization omitted for clarity.

(δ 29.96 and 11.83 (benzene-*d*₆)) slightly upfield of those observed for **4**. The ¹H and ¹³C{¹H} NMR spectra of **5** were found to be extremely complicated, especially in the aromatic regions, due to the low symmetry (*C*₁) of the complex. The ¹H and ¹³C{¹H} NMR spectra exhibited the expected resonances for the ancillary ligand and one 2,4,6-tri-*tert*-butylanilide moiety. In particular, the *NH* anilide proton of complex **5** gave rise to a singlet in the ¹H NMR spectrum at δ 4.88 with an integration of 1H (benzene-*d*₆).

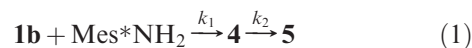
In order to unambiguously establish the connectivity of **5**, a single-crystal X-ray diffraction study was performed. Complex **5** was found to be highly crystalline in nature, and single crystals were readily obtained from a concentrated toluene solution layered with pentane at -35 °C. As depicted in the molecular structure of **5** (Figure 3), the low symmetry of the complex in the solid state (*C*₁) matched that observed in solution. The complex adopts a five-coordinate geometry with one site occupied by a 2,4,6-tri-*tert*-butylanilide ligand. The remaining four coordination sites are defined by the ancillary ligand bound in a κ^4 fashion through the three nitrogen atoms and the ortho carbon of one Pipp group. At 1.554 Å, the lutetium center sits substantially out of the plane of the dimethylcarbazole ligand backbone, presumably due to the extremely sterically demanding nature of the ligands coordinated to it. Of particular interest in complex **5** is the unusual four-membered metallacycle constituted by Lu1,

Table 2. Selected Bond Distances (Å) and Angles (deg) for Compound **5**

Lu1–N1	2.1632(32)	C39–C40	1.4083(50)
Lu1–N2	2.3072(30)	C39–N2	1.4436(46)
Lu1–N3	2.3123(30)	P1–N2	1.5840(33)
Lu1–N4	2.3122(30)	P2–N4	1.6142(31)
Lu1–C40	2.3368(42)		
N2–Lu1–N4	142.46(11)	Lu1–N2–C39	92.88(21)
N2–Lu1–N3	81.80(11)	N2–Lu1–C40	61.31(12)
N3–Lu1–N4	86.50(10)	Lu1–C40–C39	92.59(25)
N1–Lu1–N3	125.19(12)	N2–C39–C40	112.25(32)
Lu1–N1–C57	164.15(29)		

N2, C39, and C40. In the solid state the metallacycle takes on a kite-shaped geometry defined by two long bonds (Lu1–N2, 2.3072(30) Å; Lu–C40, 2.3368(42) Å) and two short bonds (C39–N2, 1.4436(46) Å; C39–C40, 1.4083(50) Å) (Table 2). The sum of the angles within the metallacycle is 359.03°, indicating a nearly planar conformation. The Lu–N1–C57 anilide bond angle in **5** (164.15(29)°) is substantially more linear than that observed in complexes **2** and **3** (which range from 143.77(65) to 151.34(17)°). This difference is likely due to the increased steric bulk of the 2,4,6-tri-*tert*-butylanilide ligand.

Kinetic Analysis. Due to its rapid rate of decomposition, complex **4** could be neither isolated nor fully characterized by ¹H or ¹³C{¹H} NMR spectroscopy. However, the formation of **4** from **1b**, followed by its decomposition to complex **5** (eq 1), was quantitatively monitored by ³¹P{¹H} NMR spectroscopy. The progress of reaction at 296.9 K (from *t* = 185 s to *t* = 157 000 s) is portrayed in Figure 4 as a stacked plot of ³¹P{¹H} NMR spectra (toluene-*d*₈) recorded at predefined time intervals. Over the course of the reaction, the decreasing concentration of **1b** (δ 29.7) is accompanied by the formation of asymmetric intermediate **4**, depicted by two signals resonating at δ 31.7 and 22.4. Within two days at this temperature, complex **4** gradually undergoes an intramolecular metalation exchange to afford exclusively product **5** (δ 29.7 and 11.4).



The observed rate constant ($k_1(\text{obsd})$) for the formation of complex **4** was obtained from a second-order plot of the reaction of **1b** with Mes*NH₂. The reaction was monitored over a broad range of temperatures (296.9–349.1 K), with observed *t*_{1/2} values ranging from 18 500 to 198 s (Table 3). An Eyring plot was constructed that allowed for extraction of the activation parameters $\Delta H^\ddagger = 73.5(2)$ kJ mol⁻¹ and $\Delta S^\ddagger = -50.3(5)$ J K⁻¹ mol⁻¹ for this transformation (Figure 5a).

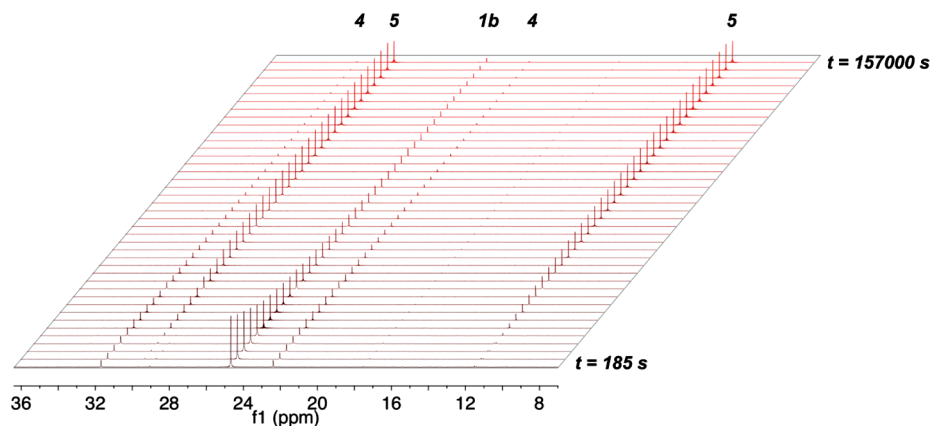


Figure 4. Stacked $^{31}\text{P}\{^1\text{H}\}$ NMR spectra depicting the metallacycle ring-opening reaction of complex **1b** to **4** followed by transformation to complex **5**.

Table 3. Observed and Calculated Rate Constants for the Metallacycle Ring-Opening Reaction of Complex **1b** with Mes^*NH_2 at Temperatures Ranging from 296.9 to 349.1 K

T/K	$k_1(\text{obsd})/\text{M}^{-1}\text{s}^{-1}$	$t_{1/2}(\text{obsd})/\text{s}$	$k_1(\text{calcd})/\text{M}^{-1}\cdot\text{s}^{-1}$	$t_{1/2}(\text{calcd})/\text{s}$
296.9	1.81×10^{-3}	18500	1.69×10^{-3}	19900
304.6	3.43×10^{-3}	9660	3.22×10^{-3}	10300
315.7	9.96×10^{-3}	3330	9.44×10^{-3}	3510
326.8	3.07×10^{-2}	1070	2.68×10^{-2}	1230
338.0	7.44×10^{-2}	445	6.42×10^{-2}	517
349.1	1.66×10^{-1}	198	1.49×10^{-1}	222

Table 4. Calculated Rate Constants for the Intramolecular Rearrangement of Complex **4** to Complex **5** at Temperatures Ranging from 296.9 to 349.1 K

T/K	$k_2(\text{calcd})/\text{s}^{-1}$	$t_{1/2}(\text{calcd})/\text{s}$
296.9	3.17×10^{-5}	21900
304.6	8.46×10^{-5}	8200
315.7	2.54×10^{-4}	2730
326.8	6.84×10^{-4}	1010
338.0	2.02×10^{-3}	342
349.1	5.14×10^{-3}	135

Table 5. Transition State Activation Parameters for the Transformation of Complex **1b** to **5**

rate const	$\Delta H^\ddagger/\text{kJ mol}^{-1}$	$\Delta S^\ddagger/\text{J K}^{-1}\text{mol}^{-1}$
$k_1(\text{obsd})$	73.5(2)	-50.3(5)
$k_1(\text{calcd})$	72.3(1)	-55.0(4)
$k_2(\text{calcd})$	80.3(1)	-60.0(4)

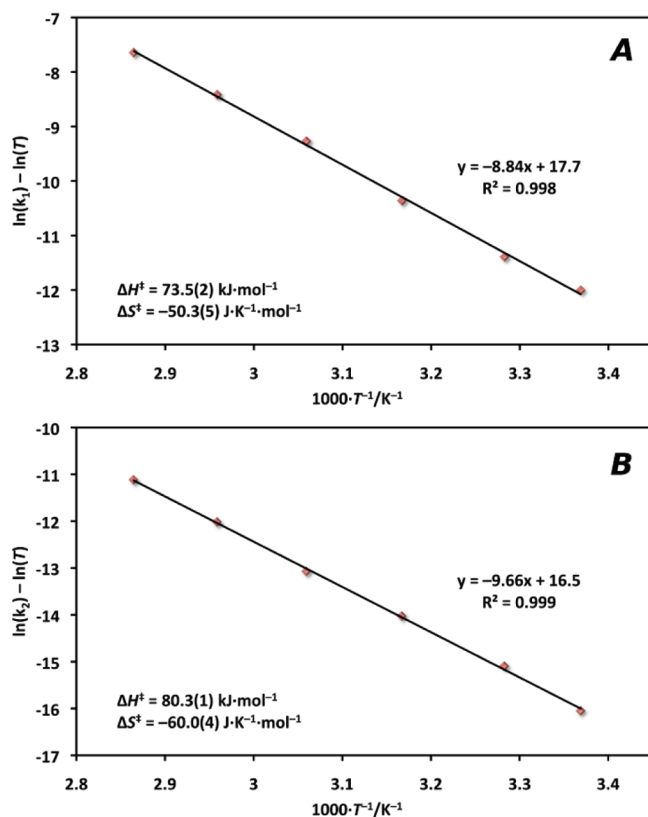


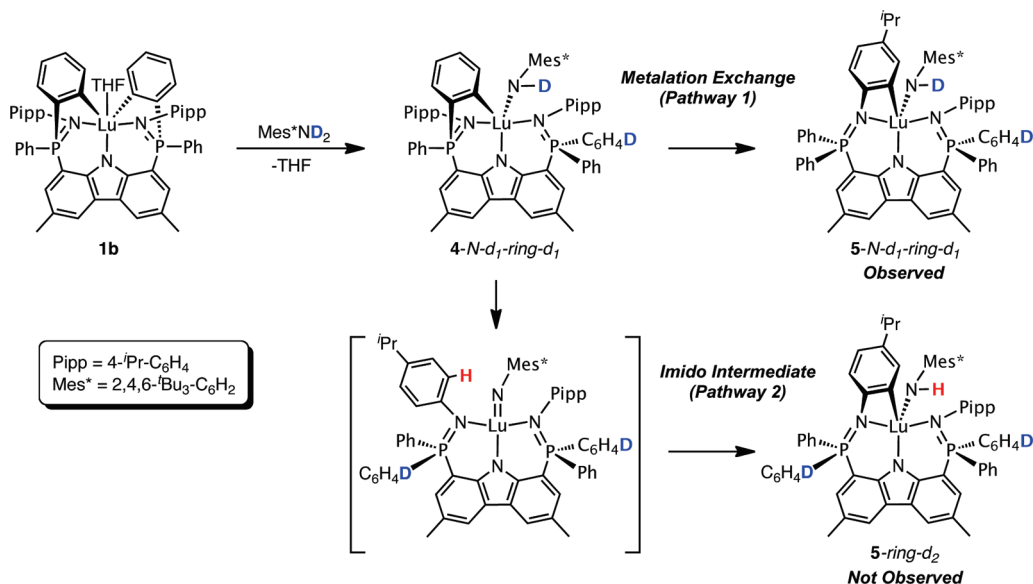
Figure 5. (a) Eyring plots for (a) the metallacycle ring-opening reaction of **1b** to **4** (derived from $k_1(\text{obsd})$) and (b) the intramolecular rearrangement of **4** to **5** (derived from $k_2(\text{calcd})$).

The large negative entropy of activation suggests a highly ordered transition state, consistent with the expected σ -bond metathesis mechanism.

In contrast to the second-order reaction which converted complex **1b** to **4**, the transformation from **4** to **5** involved significantly more complicated kinetic behavior. No simple mathematical rate law could be derived for the expression of k_2 due to the complexity of the consecutive reactions. Thus, no values for $k_2(\text{obsd})$ could be determined from the experimental data. However, using the kinetic simulation software COPASI,¹¹ we were able to model the two-step process from **1b** to **5**. As such, the modeled data set allowed for calculation of the simulated rate constants, $k_1(\text{calcd})$ and $k_2(\text{calcd})$, for the consecutive reactions; these values are listed in Tables 3 and 4, respectively. The $k_1(\text{calcd})$ values agree fairly well with the $k_1(\text{obsd})$ values; however, it should be noted that the calculated rate constants were consistently slightly slower (by 5–14%) than the observed rate constants. Due to this observation, it is reasonable to assume that the calculated rate constants for k_2 (Table 4) may also be slow by a similar margin of error. However, a visual inspection of the simulated reaction progress over time indicated good agreement with the experimental reaction plots.

As with the observed rate constant $k_1(\text{obsd})$, Eyring plots were constructed to express the temperature dependence of the simulated rate constants $k_1(\text{calcd})$ and $k_2(\text{calcd})$. From these plots, the activation parameters of $\Delta H^\ddagger = 72.3(1)$ kJ mol⁻¹

(11) Hoops, S.; Sahle, S.; Gauges, R.; Lee, C.; Pahle, J.; Simus, N.; Singhal, M.; Xu, L.; Mendes, P.; Kummer, U. *Bioinformatics* **2006**, *22*, 3067–3074.

Scheme 5. Deuterium Labeling Experiment 1: Reaction of Complex **1b** with Mes*ND₂

and $\Delta S^\ddagger = -55.0(4) \text{ J K}^{-1} \text{ mol}^{-1}$ and $\Delta H^\ddagger = 80.3(1) \text{ kJ mol}^{-1}$ and $\Delta S^\ddagger = -60.0(4) \text{ J K}^{-1} \text{ mol}^{-1}$ were extracted for $k_1(\text{calcd})$ and $k_2(\text{calcd})$, respectively (Table 5). The parameters obtained for $k_1(\text{calcd})$ agree very well with those obtained from $k_1(\text{obsd})$. For the activation parameters obtained from the $k_2(\text{calcd})$ rate constants, both the enthalpic barrier and entropy of activation remained similar to that for k_1 .

Deuterium Labeling and Mechanism. The structure of complex **5**, confirmed by solution multinuclear NMR spectroscopy and solid-state X-ray diffraction analysis, suggests that an unusual reaction mechanism is operative in its formation from starting material **1b**. It is evident that the mechanism for the generation of **5** from **1b** requires multiple steps, due to the intermediacy of **4**, as observed by multinuclear NMR spectroscopy. Several pathways for this transformation can be envisioned, the two most plausible of which will be described in depth. The first mechanism (pathway 1) involves the metallacycle ring-opening reaction of complex **1b** with Mes*ND₂ to give mono(anilide) **4**, followed by direct metalation exchange of the aryl rings between P-Ph and N-Pipp groups of the ancillary ligand to afford complex **5** as the final product. An alternative mechanism (pathway 2) could involve the formation of **4** as in pathway 1. Following this, intramolecular metallacycle ring opening of complex **4** could give rise to a transient lutetium imido complex, whereby remetalation of an N-Pipp group would afford the final product **5**. Although there have been no terminal, unconstrained lutetium imides reported to date,¹² there are several examples of rare-earth-metal complexes that are formed via a transient terminal imido intermediate.^{10,13} More recently, the isolation of a terminal scandium imide has been realized,¹⁴ thus suggesting that the paucity of such rare-earth species in the literature is not due to thermodynamic limitations. In order to establish which mechanism is operative in the formation

of **5** from **1b**, we performed two independent deuterium labeling experiments (Schemes 5 and 6).¹⁵

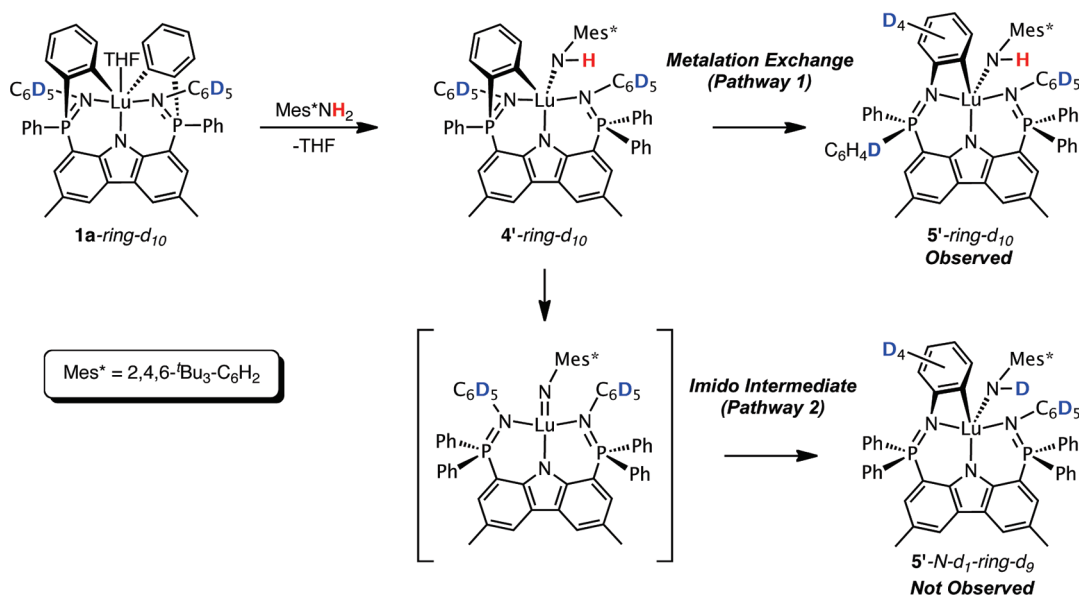
The first deuterium labeling experiment involved the reaction of complex **1b** with Mes*ND₂. As outlined in Scheme 5, if pathway 1 was operative, the labeled anilide formed upon initial reaction (**4-N-d₁-ring-d₁**) would retain a deuterium atom on the anilide nitrogen throughout the transformation to give the final product **5-N-d₁-ring-d₁**, with a deuterium-labeled anilide nitrogen. Conversely, if pathway 2 was operative, the deuterium on the anilide nitrogen of **4-N-d₁-ring-d₁** would become scrambled into the P-phenyl rings upon imido formation. This would be followed by remetalation of an N-Pipp group, thus installing a proton onto the anilide nitrogen atom of the final putative product, **5-ring-d₂**. When this reaction was followed on an NMR tube scale by ¹H NMR spectroscopy, it was determined that the final product of the transformation contained a deuterium atom on the anilide nitrogen, thus suggesting that pathway 1, rather than pathway 2, was operative. This conclusion was supported by the lack of a resonance at δ 4.88 in the ¹H NMR spectrum of

(15) Two additional mechanisms (pathways 3 and 4) have also been suggested to us. Pathway 3 involves the reaction of complex **4** with a second equivalent of Mes*ND₂ to give the bis(anilide) complex analogous to **2** and **3**. From such a species, loss of 2,4,6-tri-*tert*-butylaniline with concomitant metalation of an N-Pipp group would result in **5**. Pathway 3 is not considered to be a probable mechanism on the grounds of steric hindrance. It does not appear to be possible to fit two 2,4,6-tri-*tert*-butylanilide groups into the coordination pocket defined by the ancillary ligand because of too much steric crowding. Furthermore, operation of pathway 3 was nullified through the aforementioned deuterium labeling studies. For example, in deuterium labeling experiment 1, the reaction of **1b** with 2 equiv of Mes*ND₂ would result in the intermediate (L^{Pipp}-κ³N-ring-d₂)Lu(NDMes*)₂ if pathway 3 were operative. This species would then undergo loss of Mes*NHD to give the final product **5-N-d₁-ring-d₂**. It can be expected then that, in subsequent reactions, competition between **1b** reacting with Mes*ND₂ or Mes*NHD would occur. As a result, deuterium incorporation on the anilide nitrogen of complex **5** would not be either 100% or 0% (as for pathways 1 and 2, respectively) but, rather, a statistical mixture. In pathway 4, the anilide ligand in complex **4** could serve to shuttle an H atom from the N-Ar group to the metalated P-Ph moiety via the intermediate (L-κ³N,κ³C^{P-Ph},κ³C^{N-Ar})Lu(NH₂Mes*). This mechanism was disproven by both deuterium labeling experiments, as Mes*NHD, which would afford a statistical mixture of D and H incorporation on the anilide nitrogen of complex **5**, would be produced in both cases.

(12) (a) Giesbrecht, G. R.; Gordon, J. C. *Dalton Trans.* **2004**, 2387–2393. (b) Scott, J.; Mindiola, D. J. *Dalton Trans.* **2009**, 8463–8472.

(13) (a) Beetstra, D. J.; Meetsma, A.; Hessen, B.; Teuben, J. H. *Organometallics* **2003**, *22*, 4372–4374. (b) Conroy, K. D.; Piers, W. E.; Parvez, M. *Organometallics* **2009**, *28*, 6228–6233.

(14) Lu, E.; Li, Y.; Chen, Y. *Chem. Commun.* **2010**, *46*, 4469–4471.

Scheme 6. Deuterium Labeling Experiment 2: Reaction of Complex **1a-ring-d₁₀** with Mes**NH*₂

5-N-d₁-ring-d₁ and an aromatic region that integrated for one less proton than for **5**. Other than these details, the ¹H NMR spectrum of **5-N-d₁-ring-d₁** was identical with that of the proteo control, **5**, where the NH signal can be clearly observed at δ 4.88.

The second deuterium labeling experiment involved the reaction of fully protonated Mes**NH*₂ with a deuterium-labeled lutetium analogue to **1b**, **1a-ring-d₁₀** (Scheme 6). The starting material **1a-ring-d₁₀** contained fully deuterated N-phenyl groups as opposed to the proton-containing 4-isopropylphenyl groups in **1b**. Despite the lack of an isopropyl group in the para position of the N-aryl ring, we were confident that **1a-ring-d₁₀** would react in a manner identical with that for **1b**, excluding any kinetic isotope effects. The identical reactivity patterns and kinetic behavior of **1a** (the protonated version of **1a-ring-d₁₀**) and **1b** have been previously documented.⁹ As depicted in Scheme 6, pathway 1 dictates that the reaction of **1a-ring-d₁₀** with Mes**NH*₂ would result in the products **4'-ring-d₁₀** and **5'-ring-d₁₀**, whereby a proton is retained on the anilide nitrogen throughout the entire process. Conversely, pathway 2 would result in loss of the anilide proton upon imido formation, followed by remetalation of a deuterium-labeled N-aryl ring, thus installing a deuterium atom on the anilide nitrogen. When the transformation was followed by ¹H NMR spectroscopy, the final product of the reaction of **1a-ring-d₁₀** with Mes**NH*₂ was observed to be **5'-ring-d₁₀**, with a proton bound to the anilide nitrogen. Thus, the deuterium labeling experiment 2 corroborated the results from experiment 1, in that pathway 1 rather than pathway 2 appears to be operative.

The mechanistic work presented herein suggests that the formation of complex **5** occurs via two sequential metallacycle ring-opening reactions. The first ring opening occurs during the reaction of **1b** with Mes**NH*₂ to give complex **4**, which possesses a metalated P-phenyl ring. Complex **4** then undergoes a thermal rearrangement via a rare direct metalation exchange between an N-aryl ring and the metalated P-phenyl ring to yield the structural isomer **5**. The results from deuterium labeling experiments argue against the possibility of a transient lutetium imido species being formed as an intermediate in this transformation.

Conclusion

The process of metallacycle ring opening has been probed in detail using a doubly ortho-metallated lutetium aryl complex. While reaction of (L^{Ar}-*k*³N,*k*²C^{P-Ph})Lu(THF) with bulky anilines (MesNH₂, TripNH₂) resulted in double metallacycle ring opening to generate the corresponding bis(anilide) lutetium complexes, utilization of the extremely sterically demanding Mes**NH*₂ promoted single metallacycle ring opening to afford the mono(anilide) complex (L^{Pipp}-*k*³N,*k*C^{P-Ph})Lu(NHMes*) (**4**) exclusively. The latter product was found to be highly thermally sensitive and rapidly underwent an unusual metalation exchange process to give (L^{Pipp}-*k*³N,*k*C^{N-Pipp})Lu(NHMes*) (**5**) in high yield. Through various deuterium labeling and kinetic studies it was determined that complex **5** forms through direct metalation exchange, with no evidence of a transient imido intermediate.

In an effort to access elusive Lu=E functionalities future work will explore the reactions of complex **1** with the heavier group 15 analogues of Mes**NH*₂. These larger congeners may exhibit significantly different reactivity patterns, whereby a complex possessing a terminal lutetium–main-group multiple bond may be realized through a metallacycle ring-opening pathway.

Experimental Section

General Procedures. Unless otherwise specified, all reactions were carried out under an argon atmosphere with the rigorous exclusion of oxygen and water using standard glovebox (MBraun) or high-vacuum-line techniques. The solvents pentane, benzene, and toluene were dried and purified using a solvent purification system (MBraun) and stored in evacuated 500 mL bombs over a “titanocene” indicator. Deuterated solvents (benzene-*d*₆ and toluene-*d*₈) were dried over sodium benzophenone ketyl, degassed via three freeze–pump–thaw cycles, distilled under vacuum, and stored in glass bombs under argon. Unless otherwise specified, all solvents required for air-sensitive manipulations were introduced directly into the reaction flasks by vacuum transfer with condensation at –78 °C. For air-stable manipulations, the solvents THF, diethyl ether, and hexanes were purchased from Fisher Scientific and used without further purification. Samples for NMR spectroscopy were recorded on a 300 MHz

Bruker Avance II (Ultraschield) spectrometer (^1H 300.13 MHz, $^{13}\text{C}\{^1\text{H}\}$ 75.47 MHz, $^{31}\text{P}\{^1\text{H}\}$ 121.49 MHz) and referenced relative to either SiMe_4 through the residual solvent resonance(s) for ^1H and $^{13}\text{C}\{^1\text{H}\}$ or external 85% H_3PO_4 for $^{31}\text{P}\{^1\text{H}\}$. All NMR spectra were recorded at ambient temperature (295 K) unless specified otherwise. FT-IR spectra were recorded on a Bruker ALPHA FT infrared spectrometer with Platinum ATR sampling. Elemental analyses were performed using an Elementar Americas Vario MicroCube instrument. The reagent 2,4,6-tri-*tert*-butylaniline was purchased from Frinton Laboratories and used as received. Mes^*ND_2 was prepared via the exchange reaction of Mes^*NH_2 with D_2O under the presence of a catalytic amount of anhydrous HCl in diethyl ether. TripNH_2 , $\mathbf{1a}$,⁹ and $\mathbf{1b}$ ⁹ were prepared according to literature procedures. All deuterated solvents and aniline-*ring-d*₅ were purchased from Cambridge Isotope Laboratories. All other reagents were obtained from Aldrich Chemicals or Alfa Aesar and used as received.

($\text{L}^{\text{Ph}}\text{-k}^3\text{N}\text{Lu}(\text{NHMeS}^*)_2$) (**2**). MesNH_2 (0.151 mL, 1.07 mmol) was added to a solution of **1a** (0.531 g, 0.537 mmol) in toluene (20 mL) at ambient temperature. The resulting orange solution was stirred for 1 h, following which all volatiles were removed under reduced pressure. In a glovebox, the oily residue was washed with pentane (2×2 mL) and then dried under vacuum. The solid was taken up in hot benzene, filtered, and cooled to ambient temperature, where it was left to crystallize. After 2 days the mother liquor was decanted off, leaving a yellow crystalline solid that was washed with pentane (5 mL) and thoroughly dried in vacuo. Yield: 0.376 g (59.0%). ^1H NMR (benzene-*d*₆): δ 8.12 (s, 2H, 4,5-Cz CH), 7.71 (dd, $^3J_{\text{HP}} = 11.1$ Hz, $^3J_{\text{HH}} = 7.3$ Hz, 8H, PPh *o*-CH), 7.42 (d, 2H, $J = 17.1$ Hz, 2,7-Cz CH), 6.94–6.82 (m, 20H, aromatic H), 6.70 (m, 6H, aromatic H), 3.97 (s, 2H, NH), 2.37 (s, 6H, mesityl *p*-CH₃), 2.22 (s, 6H, Cz CH₃), 2.20 (s, 12H, mesityl *o*-CH₃). $^{13}\text{C}\{^1\text{H}\}$ NMR (benzene-*d*₆): δ 154.2 (s, aromatic *ipso*-C), 151.0 (d, $J_{\text{CP}} = 3.3$ Hz, aromatic *ipso*-C), 145.9 (d, $J_{\text{CP}} = 8.2$ Hz, aromatic *ipso*-C), 134.2 (d, $J_{\text{CP}} = 9.4$ Hz, PPh *o*-CH), 133.3 (d, $J_{\text{CP}} = 13.2$ Hz, 2,7-Cz CH), 132.1 (d, $J_{\text{CP}} = 2.5$ Hz, aromatic CH), 131.6 (d, $J_{\text{CP}} = 6.5$ Hz, aromatic CH), 131.1 (s, *ipso*-C), 129.8 (s, *ipso*-C), 129.2 (s, aromatic CH), 128.6 (d, partially obscured by solvent, $J_{\text{CP}} = 11.9$ Hz, aromatic CH), 127.7 (d, obscured by solvent, $J_{\text{CP}} = 3.5$ Hz, aromatic CH), 125.5 (d, $J_{\text{CP}} = 13.9$ Hz, aromatic *ipso*-C), 125.0 (d, $J_{\text{CP}} = 2.1$ Hz, 4,5-Cz CH), 123.4 (d, $J_{\text{CP}} = 3.8$ Hz, aromatic CH), 121.4 (s, aromatic *ipso*-C), 120.0 (s, aromatic *ipso*-C), 109.2 (d, $J_{\text{CP}} = 115.7$ Hz, aromatic *ipso*-C), 21.1 (s, mesityl *p*-CH₃), 21.0 (s, mesityl *o*-CH₃), 20.3 (s, Cz CH₃). $^{31}\text{P}\{^1\text{H}\}$ NMR (benzene-*d*₆): δ 30.55. Anal. Calcd for $\text{C}_{68}\text{H}_{64}\text{LuN}_3\text{P}_2$: C, 68.74; H, 5.43; N, 5.89. Found: C, 68.35; H, 5.41; N, 5.40.

($\text{L}^{\text{Pipp}}\text{-k}^3\text{N}\text{Lu}(\text{NHTrip})_2$) (**3**). TripNH_2 (0.214 g 0.974 mmol) was added via syringe to a solution of **1b** (0.502 g, 0.467 mmol) in toluene at ambient temperature. The orange solution was stirred for 30 min, after which all volatiles were removed under reduced pressure. In a glovebox, the residue was washed with pentane (2×2 mL) and then dried under vacuum. The solid was reconstituted in toluene (2 mL), layered with pentane, and left at -35 °C for 16 h to crystallize. The crystalline material was collected by filtration, washed with pentane, and thoroughly dried in vacuo. Yield: 0.295 g (43.9%). ^1H NMR (benzene-*d*₆): δ 8.13 (s, 2H, 4,5-Cz CH), 7.52 (dd, $^3J_{\text{HP}} = 11.2$ Hz, $^3J_{\text{HH}} = 7.1$ Hz, 8H, PPh *o*-CH), 7.44 (d, $^3J_{\text{HP}} = 17.7$ Hz, 2H, 2,7-Cz CH), 7.11 (s, 4H, Trip *m*-CH), 6.97 (ov m, $^3J_{\text{HH}} = 7.2$ Hz, 4H, PPh *p*-CH), 6.89 (ov m, 12H, PPh *m*-CH + Pipp *o*-CH), 6.56 (d, $^3J_{\text{HH}} = 7.2$ Hz, 4H, Pipp *m*-CH), 3.97 (s, 2H, NH), 3.26 (br sp, 4H, Trip *o*-CH(CH₃)₂), 3.01 (sp, $^3J_{\text{HH}} = 6.9$ Hz, 2H, Trip *p*-CH(CH₃)₂), 2.54 (sp, $^3J_{\text{HH}} = 6.9$ Hz, 2H, Pipp *p*-CH(CH₃)₂), 2.20 (s, 6H, Cz CH₃), 1.43 (d, $^3J_{\text{HH}} = 6.9$ Hz, 12H, Trip *p*-CH(CH₃)₂), 1.11 (d, $^3J_{\text{HH}} = 6.6$ Hz, 24H, Trip *o*-CH(CH₃)₂), 1.02 (d, $^3J_{\text{HH}} = 6.9$ Hz, 12H, Pipp *p*-CH(CH₃)₂). $^{13}\text{C}\{^1\text{H}\}$ NMR (benzene-*d*₆): δ 152.7

(s, aromatic *ipso*-C), 151.5 (d, $J_{\text{CP}} = 3.3$ Hz, aromatic *ipso*-C), 143.5 (d, $J_{\text{CP}} = 4.3$ Hz, aromatic *ipso*-C), 143.1 (d, $J_{\text{CP}} = 8.7$ Hz, aromatic *ipso*-C), 134.9 (d, $J_{\text{CP}} = 9.5$ Hz, PPh *o*-CH), 134.3 (d, $J_{\text{CP}} = 13.1$ Hz, 2,7-Cz CH), 132.6 (s, aromatic *ipso*-C), 132.3 (s, aromatic *ipso*-C), 131.9 (s, PPh *p*-CH), 131.9 (d, $J_{\text{CP}} = 10.4$ Hz, Pipp *o*-CH), 130.7 (d, $J_{\text{CP}} = 92.0$ Hz, aromatic *ipso*-C), 128.1 (d, $J_{\text{CP}} = 11.7$ Hz, PPh *m*-CH), 125.9 (d, $J_{\text{CP}} = 3.6$ Hz, Pipp *m*-CH), 125.4 (d, $J_{\text{CP}} = 14.1$ Hz, aromatic *ipso*-C), 125.1 (d, $J_{\text{CP}} = 3.7$ Hz, 4,5-Cz CH), 120.6 (s, Trip *m*-CH), 120.5 (s, aromatic *ipso*-C), 107.6 (d, $J_{\text{CP}} = 115.6$ Hz, aromatic *ipso*-C), 34.7 (s, Trip *p*-CH(CH₃)₂), 33.5 (s, Pipp *p*-CH(CH₃)₂), 30.2 (br s, Trip *o*-CH(CH₃)₂), 25.4 (s, Trip *p*-CH(CH₃)₂), 24.3 (s, Trip *o*-CH(CH₃)₂), 24.1 (s, Pipp *p*-CH(CH₃)₂), 21.0 (s, Cz CH₃). $^{31}\text{P}\{^1\text{H}\}$ NMR (benzene-*d*₆): δ 30.57. Anal. Calcd for $\text{C}_{91}\text{H}_{112}\text{LuN}_5\text{P}_2$ ($3 \cdot$ pentane): C, 72.25; H, 7.46; N, 4.63. Found: C, 72.33; H, 7.82; N, 4.85.

($\text{L}^{\text{Pipp}}\text{-k}^3\text{N}\text{Lu}(\text{NHMeS}^*)$) (**5**). Toluene (40 mL) was added to a bomb charged with an intimate mixture of **1b** and Mes^*NH_2 to give an orange solution. The reaction mixture was heated to 100 °C for 3 h, following which it was cooled to ambient temperature and the volume concentrated under vacuum to ~ 5 mL. Upon standing for 5 min the product crystallized out of solution as a solid orange mass. In a glovebox, the crystals were redissolved in 5 mL of hot toluene to give a dark red solution. After it was cooled to ambient temperature, the toluene solution was layered with pentane (5 mL) and left for 16 h to crystallize. Matted needles of the product were collected by filtration, washed with pentane (2×2 mL), and thoroughly dried under reduced pressure. Yield: 0.716 g (77.3%). $^1\text{H}\{^{31}\text{P}\}$ NMR (benzene-*d*₆): δ 8.02 (s, 1H, 4-Cz CH), 7.96 (ov d, $^3J_{\text{HH}} = 8.1$ Hz, 2H, PPh *o*-CH), 7.94 (ov s, 1H, 5-Cz CH), 7.84 (d, $^3J_{\text{HH}} = 7.4$ Hz, 2H, PPh *o*-CH), 7.81–7.78 (m, 2H, aromatic H), 7.56 (d, $^3J_{\text{HH}} = 8.2$ Hz, 2H, PPh *o*-CH), 7.84 (d, $^3J_{\text{HH}} = 8.3$ Hz, 2H, PPh *o*-CH), 7.39 (s, 2H, Mes* *m*-CH), 7.20 (s, 1H, 2-Cz CH), 7.14 (s, obscured by solvent, 1H, 7-Cz CH), 7.09–7.06 (m, 2H, aromatic H), 7.02–7.00 (m, 4H, aromatic H), 6.94–6.82 (m, 5H, aromatic H), 6.73 (d, 2H, aromatic H), 6.69 (d, 2H, aromatic H), 6.53 (m, 2H, PPh *m*-CH), 4.88 (s, 1H, NH), 2.83 (sp, $^3J_{\text{HH}} = 7.0$ Hz, 1H, Pipp' CH(CH₃)₂), 2.67 (sp, $^3J_{\text{HH}} = 6.8$ Hz, 1H, Pipp CH(CH₃)₂), 2.31 (s, 3H, 3-Cz CH₃), 2.17 (s, 3H, 6-Cz CH₃), 1.40 (s, 9H, *p*-^tBu), 1.36 (s, 18H, *o*-^tBu), 1.30 (d, $^3J_{\text{HH}} = 7.0$ Hz, 3H, Pipp' CH(CH₃)(CH₃)'), 1.27 (d, $^3J_{\text{HH}} = 7.0$ Hz, 3H, Pipp' CH(CH₃)(CH₃)'), 1.18 (d, $^3J_{\text{HH}} = 6.8$ Hz, 3H, Pipp CH(CH₃)(CH₃)'), 1.16 (d, $^3J_{\text{HH}} = 6.8$ Hz, 3H, Pipp CH(CH₃)(CH₃)'). $^{13}\text{C}\{^1\text{H}\}$ NMR (benzene-*d*₆): δ 182.8 (d, $J_{\text{CP}} = 21.7$ Hz, C–Lu), 154.1 (s, aromatic *ipso*-C), 151.6 (d, $J_{\text{CP}} = 2.6$ Hz, aromatic *ipso*-C), 151.0 (d, $J_{\text{CP}} = 6.9$ Hz, aromatic *ipso*-C), 150.5 (d, $J_{\text{CP}} = 3.6$ Hz, aromatic *ipso*-C), 143.0 (d, $J_{\text{CP}} = 6.2$ Hz, aromatic *ipso*-C), 142.6 (d, $J_{\text{CP}} = 1.9$ Hz, aromatic *ipso*-C), 140.0 (s, aromatic *ipso*-C), 136.5 (d, $J_{\text{CP}} = 4.2$ Hz, aromatic CH), 134.5 (d, $J_{\text{CP}} = 9.1$ Hz, aromatic CH), 134.2 (d, $J_{\text{CP}} = 10.1$ Hz, aromatic CH), 133.8 (s, aromatic *ipso*-C), 133.7 (s, aromatic *ipso*-C), 133.2 (s, aromatic CH), 133.1 (s, aromatic CH), 133.0 (s, aromatic CH), 132.9 (s, aromatic CH), 132.6 (d, $J_{\text{CP}} = 2.9$ Hz, aromatic CH), 131.7 (d, $J_{\text{CP}} = 2.8$ Hz, aromatic CH), 131.2 (d, $J_{\text{CP}} = 8.6$ Hz, aromatic CH), 131.1 (s, aromatic CH), 130.4 (s, aromatic *ipso*-C), 130.1 (d, $J_{\text{CP}} = 34.9$ Hz, aromatic *ipso*-C), 129.1 (d, $J_{\text{CP}} = 10.3$ Hz, aromatic CH), 129.0 (d, $J_{\text{CP}} = 10.7$ Hz, aromatic CH), 128.6 (d, $J_{\text{CP}} = 12.3$ Hz, aromatic CH), 128.4 (s, aromatic CH), 127.9 (s, aromatic *ipso*-C), 127.6 (s, aromatic CH), 127.5 (d, $J_{\text{CP}} = 1.1$ Hz, aromatic *ipso*-C), 127.4 (d, $J_{\text{CP}} = 1.1$ Hz, aromatic *ipso*-C), 126.8 (d, $J_{\text{CP}} = 11.3$ Hz, aromatic CH), 126.1 (d, $J_{\text{CP}} = 47.9$ Hz, aromatic *ipso*-C), 125.9 (d, $J_{\text{CP}} = 47.1$ Hz, aromatic *ipso*-C), 125.6 (d, $J_{\text{CP}} = 2.5$ Hz, aromatic CH), 125.4 (d, $J_{\text{CP}} = 2.6$ Hz, aromatic CH), 124.8 (s, aromatic CH), 124.6 (d, $J_{\text{CP}} = 90.7$ Hz, aromatic *ipso*-C), 121.3 (s, Mes* *m*-CH), 115.9 (d, $J_{\text{CP}} = 5.4$ Hz, aromatic CH), 113.2 (d, $J_{\text{CP}} = 104.4$ Hz, aromatic *ipso*-C), 111.6 (d, $J_{\text{CP}} = 112.3$ Hz, aromatic *ipso*-C), 35.0 (s, Mes* C(CH₃)₃), 34.7 (s, Pipp' CH(CH₃)₂), 34.5 (s, Mes* C(CH₃)₃), 33.7 (s, Pipp CH(CH₃)₂), 32.4 (s, Mes* *p*-C(CH₃)₃), 30.2 (s, Mes* *o*-C(CH₃)₃),

(16) Grubert, L.; Jacobi, D.; Buck, K.; Abraham, W.; Mügge, C.; Krause, E. *Eur. J. Org. Chem.* **2001**, 3921–3932.

Table 6. Summary of X-ray Crystallography Data Collection and Structure Refinement for Compounds 2, 3, and 5

	2 ^a	3 ^b	5 ^c
formula ^d	C ₇₄ H ₇₀ LuN ₅ P ₂	C ₉₁ H ₁₁₂ LuN ₅ P ₂	C ₇₄ H ₈₁ LuN ₄ P ₂
fw ^e	1266.26	1512.77	1263.34
cryst syst	triclinic	triclinic	monoclinic
space group	<i>P</i> $\bar{1}$	<i>P</i> $\bar{1}$	<i>C</i> 2/ <i>c</i>
<i>a</i> /Å	12.6755(9)	14.357(2)	32.990(3)
<i>b</i> /Å	13.9958(10)	16.959(3)	23.689(2)
<i>c</i> /Å	17.6268(13)	17.593(3)	23.446(2)
α /deg	98.9330(10)	85.737(2)	90
β /deg	98.6410(10)	74.590(2)	104.0580(10)
γ /deg	90.7270(10)	77.178(2)	90
<i>V</i> /Å ³	3052.0(4)	4026.1(11)	17774(3)
<i>Z</i>	2	2	8
<i>D</i> _{calcd} ^d /Mg m ⁻³	1.378	1.248	0.944
μ ^d /mm ⁻¹	1.718	1.313	1.179
<i>F</i> ₀₀₀	1300	1588	1.179
cryst size/mm	0.34 × 0.29 × 0.09	0.25 × 0.21 × 0.17	0.38 × 0.13 × 0.07
cryst color	yellow	yellow	yellow
cryst habit	plate	prism	prism
θ range/deg	1.63–27.10	1.73–25.03	1.79–27.10
<i>N</i>	43225	47761	123715
<i>N</i> _{ind}	13380	14118	19565
completeness to $\theta = 27.10^\circ$ /%	99.4	99.3	99.8
<i>T</i> _{max} ; <i>T</i> _{min}	0.8677; 0.5887	0.7456; 0.5673	0.9210; 0.6628
no. of data/restraints/params	13 380/0/755	14 118/0/910	19 565/1/745
GOF on <i>F</i> ²	1.046	0.948	[0.942]
R1 ^e (<i>I</i> > 2 σ (<i>I</i>))	0.0219	0.0731	[0.0449]
wR2 ^f (<i>I</i> > 2 σ (<i>I</i>))	0.0523	0.1486	[0.1119]
$\Delta\rho_{\max}$ and $\Delta\rho_{\min}$ /e Å ⁻³	0.947; -0.363	4.515; -1.416	[2.391; -0.668]

^a Crystallized with one molecule of benzene in the asymmetric unit. ^b Crystallized with one molecule of pentane in the asymmetric unit. ^c Crystallized with two highly disordered molecules of pentane in the asymmetric unit, which were removed from the reflection file using the SQUEEZE subroutine of PLATON; statistics following treatment of data with SQUEEZE are listed in brackets. ^d For non-SQUEEZED data. ^e $R1 = \sum ||F_o| - |F_c|| / \sum |F_o|$. ^f $wR2 = \{ \sum [w(F_o^2 - F_c^2)^2] / \sum [w(F_o^2)^2] \}^{1/2}$.

25.3 (s, Pipp' CH(CH₃)(CH₃')), 24.8 (s, Pipp' CH(CH₃)(CH₃')), 24.4 (s, Pipp CH(CH₃)(CH₃')), 24.3 (s, Pipp CH(CH₃)(CH₃')), 21.4 (s, Cz CH₃). 21.3 (s, Cz CH₃). ³¹P{¹H} NMR (benzene-*d*₆): δ 30.01 (s, 1P, PippN=PPh₂), 11.85 (s, 1P, Pipp'N=PPh₂). Anal. Calcd for C₇₄H₈₁LuN₄P₂: C, 70.35; H, 6.46; N, 4.43. Found: C, 70.17; H, 7.12; N, 4.43.

Phenyl-*d*₅ Azide. Aqueous 8 M HCl (30 mL) was added dropwise in air to a clear yellow solution of aniline-*ring-d*₅ (2.52 g, 25.7 mmol) in THF (100 mL) at 0 °C. The pale yellow solution was stirred for 15 min, following which a solution of NaNO₂ (1.95 g, 28.3 mmol) in H₂O (16.5 mL) was added dropwise over 10 min. Urea (0.253 g, 4.21 mmol) was added as a solid to remove excess nitrous acid. A solution of NaN₃ (1.85 g, 28.4 mmol) in H₂O (15 mL) was added over 30 min at 0 °C, after which the cloudy white solution was stirred at this temperature for a further 1.75 h. The product was extracted into hexanes (3 × 50 mL), and the combined organic layers were washed with 1 × 50 mL of 1 M HCl, dried over MgSO₄, and concentrated in vacuo to give a yellow liquid. The product was purified by passage through a silica column (20 cm), with hexanes as eluent. The solvent was removed from the eluent by rotational evaporation, leaving the product as a canary yellow liquid. Yield: 2.66 g (83.5%). ¹³C NMR (CDCl₃): δ 140.0 (s), 129.4 (t, ¹*J*_{CD} = 24.5 Hz), 124.5 (t, ¹*J*_{CD} = 24.4 Hz), 118.7 (t, ¹*J*_{CD} = 24.3 Hz). IR: ν (cm⁻¹) 2276 (vw), 2109 (s), 2094 (s), 2034 (w), 1560 (m), 1409 (vw), 1370 (s), 1302 (vw), 1260 (s), 1098 (w), 1068 (vw), 1040 (vw), 958 (vw), 876 (vw), 841 (vw), 818 (w), 775 (vw), 753 (w), 650 (m), 625 (m), 590 (vw), 547 (s), 530 (m), 425 (s). The spectroscopic analysis of this compound agrees with previously published data for phenyl-*d*₅ azide.¹⁷

HL^{Ph}-*d*₁₀. This compound was prepared in a manner identical with that previously described for HL^{Ph},⁹ with the exception that phenyl-*d*₅ azide was used in place of phenyl azide. The ¹H and ³¹P{¹H} NMR spectra matched that previously described,

with the exception that no resonances were observed for the deuterated N-aryl groups.

(L^{Ph}- κ^3 N κ^2 C^{P-Ph})Lu(THF)-*d*₁₀ (1a-*ring-d*₁₀). This compound was prepared in a manner identical with that previously described for **1a**,⁹ with the exception that HL^{Ph}-*d*₁₀ was used in place of HL^{Ph}. The ¹H and ³¹P{¹H} NMR spectra matched those of **1a**, with the exception that no resonances were observed for the deuterated N-aryl groups.

NMR Kinetics. The rate constants *k*₁ and *k*₂ were determined by monitoring the ³¹P{¹H} NMR resonance(s) over the course of the reaction (to at least 3 half-lives) at a given temperature. In a typical experiment, **1b** (0.0163 g, 0.0152 mmol) and 2,4,6-tri-*tert*-butylaniline (0.0040 g, 0.0152 mmol) were added to a Wilmad NMR tube that was then sealed with a rubber septum (Sigma-Aldrich) and Parafilm. The tube was cooled to 0 °C, and 0.5 mL of toluene-*d*₈ was injected via syringe. The tube was removed from the cold bath and shaken briefly to mix the reagents. The tube was then immediately inserted into the NMR probe, which was pre-equilibrated to the appropriate temperature. The sample was allowed to equilibrate at the set temperature over the course of shimming the tube in the magnet. ³¹P{¹H} NMR spectra were recorded at preset time intervals until the reaction had progressed to at least 3 half-lives. The extent of reaction at each time interval was determined by integration of the peak intensity of the starting material relative to that of the intermediate and final product. An appropriately long delay between scans was utilized to ensure that integration was quantitative and not affected by the *T*₁ relaxation times of the reacting species. The observed rate constant *k*₁(obsd) was determined according to the law of mass action. The simulated rate constants *k*₁(calcd) and *k*₂(calcd) were deduced using the program COPASI.¹¹ A summary of the observed and calculated rate constants and half-lives are given in Tables 3 and 4 for *k*₁ and *k*₂, respectively.

X-ray Crystallography. Recrystallization of compound **2** from a concentrated benzene solution layered with pentane at 295 K, **3** from a concentrated pentane solution at 295 K, and **5** from a concentrated toluene solution layered with pentane at

238 K afforded single crystals suitable for X-ray diffraction. Crystals were coated in dry Paratone oil under an argon atmosphere and mounted onto a glass fiber. Data were collected at 173 K using a Bruker SMART APEX II diffractometer (Mo K α radiation, $\lambda = 0.71073$ Å) outfitted with a CCD area detector and a KRYO-FLEX liquid nitrogen vapor cooling device. A data collection strategy using $\omega-2\theta$ scans at 0.5° steps yielded full hemispherical data with excellent intensity statistics. Unit cell parameters were determined and refined on all observed reflections using APEX2 software.¹⁸ Data reduction and correction for Lorentz-polarization were performed using SAINT-Plus software.¹⁹ Absorption corrections were applied using SADABS.²⁰ The structures were solved by direct (2) or Patterson (3, 5) methods and refined by the least-squares method on F^2 using the SHELXTL software suite.²¹ All non-hydrogen atoms were refined anisotropically. Hydrogen atom positions were calculated and isotropically refined as riding models to their parent atoms, with the exception of the anilide protons in **2** (H1N and H2N) and **5** (H1N), which were located on the Fourier map and

refined freely. No decomposition was observed during data collection. Table 6 provides a summary of selected data collection and refinement parameters. Note: In the refinement of **5**, disordered solvent molecules were removed from the reflection file using the SQUEEZE subroutine of the PLATON program.²² Reduced residuals were observed in the final SQUEEZED structure, confirming that the uncertainty in the model was a result of the disordered solvent.²³

Acknowledgment. P.G.H. acknowledges financial support from the Natural Sciences and Engineering Research Council (NSERC) of Canada for a Discovery Grant and the Canada Foundation for Innovation for a Leaders Opportunity Grant. We wish to thank Dr. Marc R. Roussel for useful discussions regarding the kinetic analysis, Mr. Tony Montana for expert technical assistance, and Mr. Craig A. Wheaton for performing elemental analyses.

Supporting Information Available: CIF files giving X-ray crystallographic data for **2**, **3**, and **5**. This material is available free of charge via the Internet at <http://pubs.acs.org>.

-
- (18) APEX2, version 2.1-4; Bruker AXS, Madison, WI, 2006.
(19) SAINT-Plus, version 7.23a; Bruker AXS, Madison, WI, 2004.
(20) Sheldrick, G. M. SADABS, version 2004/1; Bruker AXS, Madison, WI, 2004.
(21) Sheldrick, G. M. *Acta Crystallogr., Sect. A: Found. Crystallogr.* **2007**, *A64*, 112–122.

-
- (22) Spek, A. L. *J. Appl. Crystallogr.* **2003**, *36*, 7–13.
(23) Sudik, A. C.; Millward, A. R.; Ockwig, N. W.; Côté, A. P.; Kim, J.; Yaghi, O. M. *J. Am. Chem. Soc.* **2005**, *127*, 7110–7118.